The effects of P–T changes on intermolecular interactions in crystal structure of iodoform

The effects of P-T changes on intermolecular interactions in crystal structure of iodoform

Federica Bertolotti,[*a,c] Nadia Curetti,[b,c] Piera Benna[b,c] and Giuliana Gervasio[a,c]

[a] Dipartimento di Chimica, University of Turin, Via P. Giuria n°7, 10125 Turin, Italy.
[b] Dipartimento di Scienze della Terra, University of Turin, Via Valperga Caluso n°35, 10125 Turin, Italy.
[c]Centro Interdipartimentale di Cristallografia Diffrattometrica (CrisDi), Via P. Giuria n° 7, 10125 Turin, Italy. E-mail: federica.bertolotti@unito.it; tel.: +390116707504.

Abstract
The structural transition at different pressures of the halogen and hydrogen bonded molecular structure (iodoform, CHI_3) is described. The pressures analyzed up to sample decomposition are 0.85 GPa (**P1RT**) and 2.15 GPa (**P2RT**); also room conditions (**P0RT**) and low temperature (106 K, **P0LT**) structures have been reported for comparison. The observed disorder-order phase transition, from $P6_3/m$ to $P6_3$ space group, can be rationalized by the intermolecular interaction analysis. The shortening of the distances among iodoform planes, observed during the compression and the temperature decreasing, determines an ordering of molecular dipoles in a parallel arrangement: this phase transition causes a shortening of I···I halogen bondings. The *BSSE* corrected cohesive energies have been calculated for all structures at DFT/B3LYP level of theory using a periodic boundary condition code and the Grimme dispersion correction. Hirshfeld surfaces and electrostatic potential mapped on charge density isosurfaces have been computed and their features have been analyzed, in order to better understand the halogen intermolecular interactions that control the structural modification of iodoform crystal.

Keywords: high pressure X-ray diffraction, halogen bonding, electrostatic potential, Hirshfeld surfaces.

Introduction

Polar and/or non-centrosymmetric crystals of organic materials are highly requested because they can
be used as optoelectronic transducers, actuators, ferro-, piezo and pyroelectric materials and for technological applications [1].
Iodoform (CHI_3) is a good molecule in this sense, with permanent dipole moment and a rigid molecular arrangement [2]. As well as many crystals characterized by charge transfer interactions, it has well known non linear optical properties and it shows a wide range of applications in the synthesis of novel chemical products and polymers [3].
The applicability of this powerful material is strongly connected to the range of thermodynamic stability of its chiral crystal structure; about this peculiar property a lot of work has been done: the early X-ray diffraction studies at room temperature and pressure have suggested that it belongs to the
chiral space group P63 [4], although a neutron diffraction experiment has shown a disordered structure refined in the P63/m space group [5]. Almost all solid state spectroscopic studies of CHI3 have been interpreted in term of polar structure; reports showing the anomalous behavior of lattice modes intensities have suggested a phase transition at 260 K [6]. About the behavior of iodoform crystal structure under pressure, recently X-ray powder diffraction experiments indicate no phase transitions up to 40GPa [3]. A recent X–ray single crystal study at 106 K has shown a

P63 structure [7]. At our knowledge no attempts have been made to study CHI3 crystal structure at variable pressure using single crystal X-ray diffraction techniques and Diamond Anvil Cell (DAC) as a tool to freeze the structure at different pressures.

The crystal is built up of layers of molecules perpendicular to [001] direction; the halogen···halogen

interactions form intra- and inter-layers bondings and hydrogen bonds contribute to the links among

planes. Figure 1 shows the antiparallel/ parallel molecules of the disordered P63/m structure and the

parallel packing of molecules in the $P6_3$ space group.

Pressure is well-known for suppressing structural disorder [8] and the aim of our study is to analyze

the trend of structural changes in the title compound. The main effects of pressure on a chemical

system involve changes in the interatomic distances (elastic- reversible or plastic-irreversible) and in

the phenomena related to the redistribution of electron density. Since organic molecules are usually not spherically symmetric, their rotations in the structure and the changes in the bond lengths and in bond and torsion angles increase the number of possible variants of pressure-induced structural changes; the weak bondings are more influenced by pressure changes. As a result, one can observe either a structural reconstruction (a phase transition) or a continuous distortion within the limits of stability of the same phase [9].

Our structural approach allows to deepen the CHI3 crystal structure in order to explore the behavior

of its intermolecular interactions, as well as their stability and compressibility under different pressuretemperature conditions. The changing of hydrogen bond in CHI3 under pressure has already been analyzed using powder XRD [3], but further information on halogen and hydrogen bonds can be

achieved using the experimental approach of the present work.

Figure 1. Iodoform in $P6_3/m$ ***(a)*** and $P6_3$ ***(b)*** packing.

a)

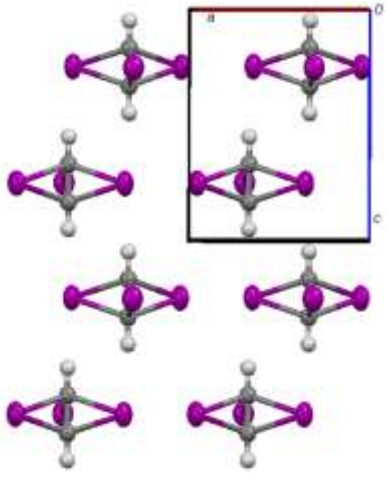

b)

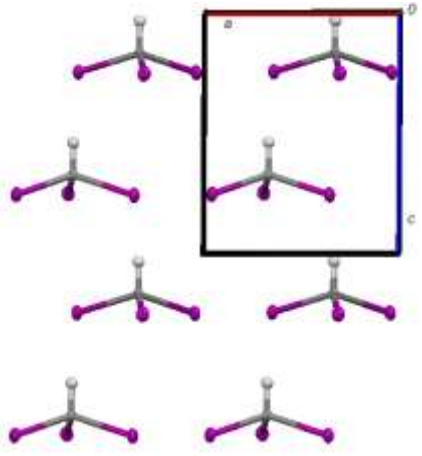

Experimental

Single crystal X-ray diffraction. Yellow single crystals of iodoform (CHI_3) of suitable size have been grown from an ethylic ether solution. One crystal was used for data collection at standard conditions (**P0RT**). Two small crystals (**P1RT** and **P2RT**) were selected for high-pressure structural studies and loaded in an ETH-type diamond anvil cell (DAC) [10] for X-ray diffraction measurements. The unusual choice of using different crystals during a high pressure experiments derive from the well known low photo- and air- stability of iodoform crystals. These drawbacks have partially been avoided into the DAC hydrostatic medium, but unfortunately not completely: for this reason the crystal has been changed after each data collection, in order to save the accuracy of the measurements. A foil of T301 steel 250 μm thick was used as a gasket to hold the crystals and it was pre-indented to a thickness of 100 μm (**P1RT**) and 80 μm (**P2RT**) before drilling a hole by spark-erosion (Ø 250 μm). The cell was loaded with an oil equivalent to one used previously in literature [11] (SANTOVAC 5) as pressure-transmitting medium.

The ruby fluorescence method was used for *in situ* pressure measurement. The internal pressure was

checked with Horiba-Jobin micro-Raman spectrometer [12] by the fluorescence line shift of three rubies scattered in the hole of the DAC cell [~~13~~]. Uncertainty on *P* was estimated to be about 0.1 GPa [13]. The pressure of the experiments are: P = 0.85 GPa

(**P1RT**) and P = 2.15 GPa (**P2RT**). The single crystal X-ray data have been collected on a Gemini R

Ultra diffractometer [14] equipped with a Ruby CCD detector. A total of 2115 frames (width 0.2°, exposure time = 60 s per frame, detector-sample distance 80 mm) were collected at each pressure in

four φ- and twelve ω-scans, covering the whole accessible reciprocal space. The 171.35.21 version of

CrysAlysPro software [15] has been used for data collection and reduction. Before integration the diamonds reflections were rejected. Using Absorb-6.0 program [16] the absorption and gasket shadowing corrections have been performed. All structure have been solved by direct methods and
refined by full-matrix least-squares on F^2 using SHELX-97 package [17]. The **P1RT** and **P2RT** refinement has given reliable results in P63 space group.
The data at standard conditions (**P0RT**) have been refined in the $P6_3/m$ space group, owing to the disorder (50%) of the CH group with respect to the I_3 plane. The space group $P6_3/m$ refinement leads to a significant decrease of *R* factors with respect to the $P6_3$ refinement (from 0.0254 to 0.0205) and agrees with previous neutron diffraction experiments [18]. The test proposed by Hamilton [19], in order to choose among different refinement models, has been used to strengthen the attribution of the space group of **P0RT**, **P1RT** and **P2RT**.
The hydrogen atoms have been found in difference Fourier maps of the three refinements and the z
coordinate has been refined; a constrain has been applied to the Uiso (1.2 times the U_C). In **P0RT** all
non-hydrogen atoms have been anisotropically refined. In **P1RT** and **P2RT** only the iodine atoms have been anisotropically refined, owing to the reduced 2θ angles accessible outside the DAC and the not completely avoided interferences caused by the gasket diffraction rings and diamonds peaks. Data at 106 K and atmospheric pressure are also reported for comparison [7].
Details of the data collections and refinements are reported in Table 1.

Table 1. Experimental details[a] of **P0RT**, **P1RT** and **P2RT** measurements and refinements.

	P0RT	**P1RT**	**P2RT**
compound formula	CHI_3	CHI_3	CHI_3
compound colour	yellow	yellow	yellow
M_r	393.72	393.72	393.72
space group	$P6_3/m$	$P6_3$	$P6_3$
crystal system	hexagonal	hexagonal	hexagonal
***a*/Å**	6.811(2)	6.6601(7)	6.5551(1)
***c*/Å**	7.553(2)	7.23(3)	6.9850(1)
V/Å^{-3}	303.44(15)	277(1)	259.929(4)
Z	2	2	2
D_{calc}/g cm^{-3}	4.309	4.710	5.030
***F*(000)**	332.0	332.0	332.0
λ/Å	Mo Kα/0.71073	Mo Kα/0.71073	Mo Kα/0.71073

temperature/K	room	room	room
pressure/GPa	atmospheric	0.85	2.15
μ (Mo- Kα)/mm^{-1}	15.29	16.72	17.85
crystal size/mm	0.08×0.09×0.16	0.031×0.040×0.054	0.09×0.13×0.14
transmission coefficients range	0.252-0.396	0.273- 0.332	0.291- 0.364
θ range/ deg	3.45-26.34	3.53- 30.92	3.59-26.18
no. reflections	3355	1383	682
no. of unique reflections	227	137	142
	-8 < *h* <8	-9 < *h* < 9	-8 < h < 8
***hkl* range**	-8 < *k* < 8	-9 < *k* < 9	-6 < k < 6
	-9 < *l* < 9	-2 < *l* < 3	-8 < l < 8
R_{int}	0.0711	0.1526	0.454
R_σ	0.0224	0.0630	0.1944
no. of refined parameters	13	12	12
R [$F_o > 4\sigma(F_o)$]	0.0213	0.0516	0.1007
wR [$F_o > 4\sigma(F_o)$]	0.0691	0.1056	0.2299
goodness of fit, S	1.112	1.052	1.084
LS extinction coefficient	0.012	/	/
residual peaks/eÅ^{-3}	-0.75/0.52	-0.52/0.55	-1.485/3.237
max shift/esd. in last cycle	< 10^{-3}	< 10^{-3}	< 10^{-3}

[a] $R=\Sigma(||F_o|-|F_c||)/\Sigma|F_o|$; $R_w = \{\Sigma[w(F_o-F_c)^2]/\Sigma w(F_o)^2\}^{1/2}$ (where w is the SHELX-97 weighting scheme: $w=1/[\sigma^2(F_o^2)+(aP)^2+bP]$ where $P=(\mathrm{Max}(F_o^2,0)+2\cdot F_c^2)/3$ and a and b are empirical terms); $R_{int}=\Sigma[n/(n-1)^{1/2}\ |F_o^2-F_o^2(\mathrm{mean})|/\ \Sigma F_o^2$; $R_\sigma=\Sigma[\sigma(F_o^2)/\ \Sigma(F_o^2)]$; $S=\{\Sigma[w(F_o^2-F_c^2)]/(n_{obs}-n_{par})\}^{1/2}$

Computational details. Kohn-Sham DFT [20] method is now most widely used for electronic calculation in condensed matters physics and in quantum chemistry. However a general drawback of
all common Density Functionals (including hybrids, as the most popular B3LYP) is that they cannot
describe long range electron correlation, responsible of the dispersion forces in van der Waals crystals [21]. To overcome this problem different strategies have been proposed: among them the Grimme empirical correction to DFT methods for molecular systems [22] has been implemented in *CRYSTAL09* code [23], the periodic *ab initio* software used for iodoform cohesive energy computing.
For iodine an all electron double zeta valence (DZV) quality basis set plus polarization functions [24]
have been used after a re-optimization of some Gaussian exponents and a standard 31.50 Jnm$_6$ mol$_{-1}$
C_6 coefficient, as proposed by Grimme [21]. For carbon and hydrogen atoms a 6-311G(*d*) and a 3-11G(*p*) basis sets have been used respectively with C_6(C) = 1.75 Jnm$_6$ mol$_{-1}$ and C_6(H) = 0.14 Jnm$_6$
mol$_{-1}$. For all calculations the truncation criteria for bielectronic integrals has been set to 7 7 7 7 18,

the shrinking factor of the commensurate reciprocal space grid was set at 8, corresponding to 60 independent *k*-vectors in the irreducible Brillouin zone. Computed cohesive energies at experimental
geometries have been corrected for the *Basis Set Superposition Error* (*BSSE*) through the Boys-Bernardi counterpoise method (*CP*) [25].

Results and Discussion

Phase transition. As expected, **s**ignificant structural changes have been observed with respect to **P0RT**, decreasing the temperature (**P0LT**) or increasing the pressure (**P1RT** and **P2RT**) at room temperature. Decreasing the temperature up to 106 K, as already shown by Raman temperature dependent experiments [11], the transition is observed from a disordered $P6_3/m$ crystal structure to a
$P6_3$ structure in which the more favoured parallel orientation of the dipole moments of molecules prevails and the mirror pseudo-symmetry disappears. The same behaviour has been shown freezing the
iodoform molecules at different pressures. Increasing pressure and decreasing temperature the distances among the iodine planes gradually decrease (Figure 2) and an additional stabilization through the formation of gradually stronger halogen and hydrogen bonds occurs (see below). In the isostructural $CHCl_3$ and $CHBr_3$ [26], the non-centrosymmetric and polar space group is maintained for all range of pressure investigated, up to 0.75GPa.

Figure 2. Variation of distances among I_3 planes in iodoform crystal structure. Squares and triangle show the data of **P0RT**, **P1RT**, **P2RT** and **P0LT** respectively.

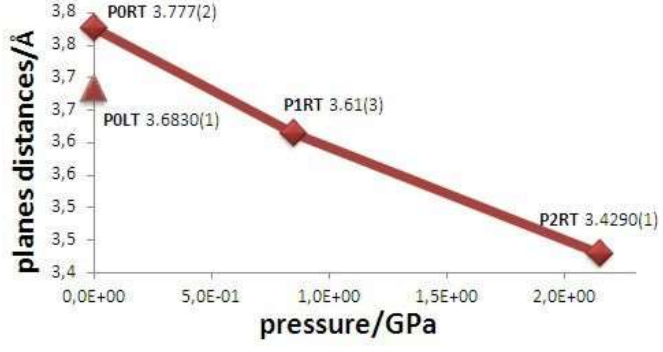

Structural changes induced by pressure and temperature. Figure 3 shows the monotonic behaviour of the cell parameters with pressure. As expected on the basis of Birch-Murnagham equation of state, cell parameters slowly decrease increasing pressure. The same effect has been found decreasing the temperature, due mainly to the reduced thermal motion of atoms that causes a more compact structure. Analyzing lattice parameters modifications under different pressures applied, *c/a* ratio always remains close to unit in the pressure range analyzed, although it slightly decrease increasing pressure: this can be ascribed to the little modification of the elastic properties

of the crystal under compression and the same result up to 2.2 GPa has been shown in reference [3] through powder diffraction experiments.

Figure 3. Evolution of lattice parameters as a function of pressure for iodoform. Squares and triangles show the data of **P0RT**, **P1RT**, **P2RT** and **P0LT** respectively**.**

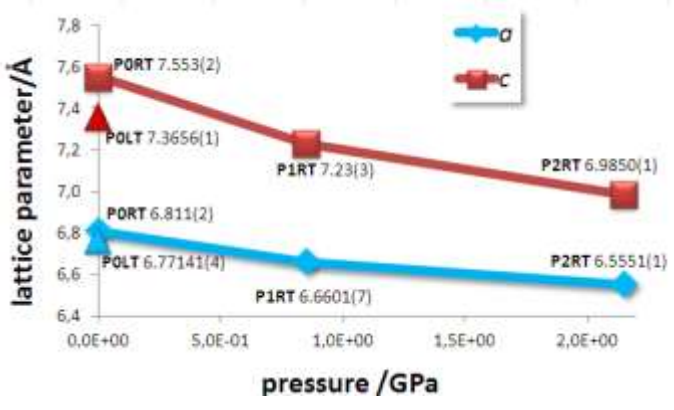

The main interactions in crystal packing of iodoform are the halogen I···I bondings and secondly the
weak H···I interactions; the halogen bondings keep together the molecules in planes perpendicular to c axis and act also among the planes. The hydrogen bondings instead occur only among the planes.
The analysis of the intermolecular contacts can be made using the Hirshfeld surfaces. The Hirshfeld surface is defined as the boundary of the region where "the electron distribution of a sum of spherical atoms for the molecule (the promolecule) dominates the corresponding sum over the crystal (the procrystal)"[27]. A range of properties can be mapped onto the Hirshfeld surface in order to display information about the surface. Each molecule in the asymmetric unit of a given crystal structure has a unique Hirshfeld surface, enabling a direct comparison between molecules in different chemical environments. Recent developments in the programs enable mapping of distances normalized using atomic van der Waals radii (d_{norm}) onto the surface and to analyze the types of interactions individually, both using the Hirshfeld surface and the corresponding fingerprint plot [28]. Hirshfeld
surfaces have been calculated using *CrystalExplorer 2.1* [29]. In Figure 4 d_{norm} values mapped on Hirshfeld surface for **P2RT** packing are shown; it is remarkable the high positive red values of d_{norm} in correspondence of I and H atoms punto fine frase

Figure 4. Hirshfeld surface for **P2RT** crystal structure. The surface points with intermolecular contacts shorter than the van der Waals sum are red, longer contacts are blue and contacts around the sum are white.

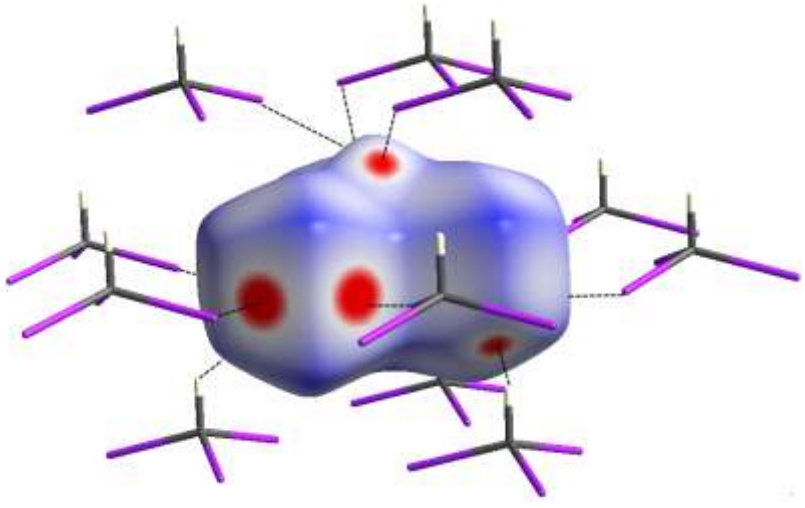

Halogen bonding features. Halogen bonding is the well-known non-covalent interaction where halogen atoms function as electrophilic and nucleophilic species. This strong, directional and selective interaction, highly electrostatic in nature, although less explored than hydrogen bond has already been used in crystal engineering of solid state materials for various applications: e.g. to direct the selfassembly of non-mesomorphic component into supramolecular liquid crystals, to control the structural and physical properties of conducting and magnetic molecular materials, to separate mixture of enantiomers, to afford and tune the second order non-linear optical responses and for biomimetic reactions [30]. Several quantum chemical investigations has shown the "amphoteric" character of halogen atoms: the electron density around covalently bound halogens is anisotropically distribute with a belt of charge density in the equatorial region and an area of its depletion (the σ-hole, due to the electron deficient outer lobe of an half- filled *p* bonding orbital) at the top of halogen atom. This charge density distribution, so called "polar flattening" explains why the nature and the strength of halogen···halogen interaction strongly depends on its geometry.

Scheme 1. Definition of θ_1 and θ_2 angles in halogen interactions.

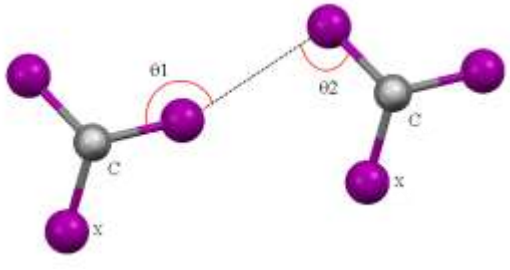

According to earlier studies, there are two distinct types of angular preferences for C–X1···X2–C (X=
halogen) interactions (Scheme 1): *i)* type-I interactions in which θ1≈θ2≈140°-180° and almost always symmetrical around a crystallographic inversion center and *ii)* type-II halogen bonds with θ1≈180°, θ2≈90° commonly associated with crystallographic screw axis and glide planes [31].

This experimental evidence can be stressed not only on geometrical point of view but also on the basis of charge density distribution considerations [32]. In interaction type-I the dispersion term of the interaction energy prevails on the electrostatic one; it cannot be considered as repulsive interaction, because it is responsible of the packing of a large number of organic crystals [30]. Looking at Laplacian of charge density distribution in molecular crystals containing halogen bondings, in type-II interaction the nucleophilic area of electron concentration of an halogen atom (nucleophile) "looks" to a charge depletion area of a neighbor (the Lewis acid); this kind of halogen bonding can be considered as “peak to hole” interaction or Lewis type. The type-II interaction is clearly responsible of the triangular X_3 interactions lying in I_3 planes (in yellow and green in Figure 6) and it represents the main interaction pattern in iodoform crystal packing and it is a synthon used in structural design [33].

Figure 5. I_3 intermolecular triangles in iodoform crystal structure.

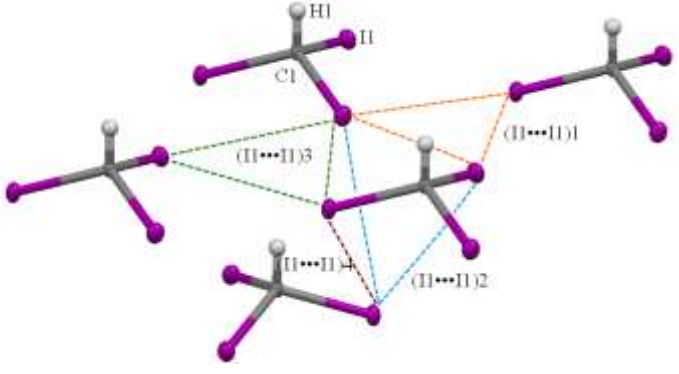

In Table 2 the most important I···I intermolecular interactions are shown. From Table 2 it is possible to assess the type of interactions confirmed also using electrostatic potential distribution mapped on a
charge density isosurface, reported in Figure 6, where the electrostatic nature of interaction type II is
clear. Changing pressure halogens bond lengths show a monotonic behavior.

Table 2. Selected intra- and intermolecular bond lengths (Å) and angles (deg.) in CHI_3 crystal structure.

	measure type		
P0RT	**P0LT [Errore. Il segnalibro non è definito.]**	**P1RT**	**P1RT**

C1–I1	2.140(4)	2.142(1)	2.12(7)	2.12(7)
$(I1\cdots I1)_1$ type II	3.940(1)	3.872(1)	3.819(2)	3.738(4)
$(I1\cdots I1)_2$ type I	4.352(2)	4.308(1)	4.196(2)	4.064(5)
$(I1\cdots I1)_3$ type II	4.409(1)	4.338(1)	4.23(1)	4.106(1)
$(I1\cdots I1)_4$ type I	4.451(1)	4.390(1)	4.29(1)	4.169(3)
$(\theta1;\theta2)_1$	154.8; 100.4	155.4; 100.8	154.7; 99.0	154.0; 97.3
$(\theta1;\theta2)_2$	94.9; 103.8	94.6; 104.4	92.3; 106.2	90.0; 108.1
$(\theta1;\theta2)_3$	145.0; 88.9	144.2; 87.8	145.4; 88.4	145.8; 88.3
$(\theta1;\theta2)_4$	93.7; 64.9;	92.3; 64.5	90.7; 65.3	88.4; 65.4

Figure 6 . Electrostatic potential in kJ mol^{-1} computed on 0.01e/$bohr^3$ charge density isosurface of CHI_3 molecule. Colors: red more positive than 301.7, 301.7 > yellow > 208.8, 208.8 > green > 115.90 and blue less than 115.90. The $(I1\cdots I1)_1$ interaction of Table 2 is reported. Red zone correspond to the σ-hole and the blue region to the negative belt.

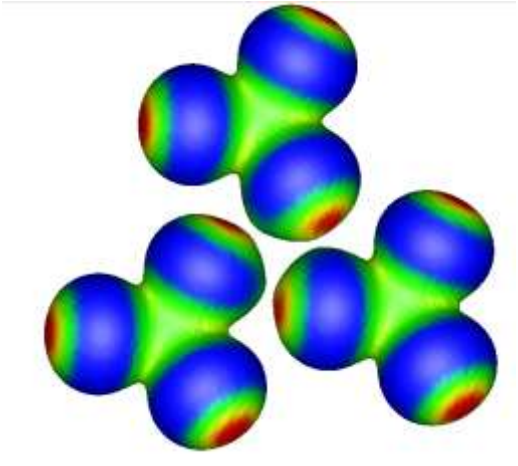

Quantitative analysis of molecular electrostatic potential. The electrostatic potential (*Vs*(**r**)) can be considered an effective tool for analyzing and predicting non-covalent interactions [32] and it has been computed on the 0.001e/bohr3 isosurface of iodoform molecules. Analyzing the values of critical points of *Vs*(**r**) under different thermodynamic conditions of CHI3, it is possible to verify how the values at σ-holes of iodine atom and on the apical hydrogen atom significantly change (Table 3). In Table 3 *Vs*(**r**) is characterized by some statistical quantities, its local maxima (*Vs,max*) and its average absolute deviation Π; *Vs,max* and *Vs,min* correlate donating and accepting tendencies respectively in halogen/hydrogen bonds and Π is a measure of internal molecule charge separation, found even in molecules with zero dipole moment. The magnitude of Π typically ranges about 8-12 kJ mol-1 in alkane hydrocarbons and 80-100 kJ mol-1 for highly polar molecules such as H2O [34]; the values of *Vs,max* and Π have a key role in our analysis. In Figure 8 the *Vs*(**r**) of CHI3 molecule is shown. Around each iodine the green-blue area corresponds to its negative belt. The *Vs*(**r**) critical points are superimposed to the surface: black points are the maxima of electrostatic potential (see Table 3), while the light blue the minima.

Table 3. Computed $V_{s,max}$ and Π in iodoform molecule under different P-T conditions, using WFA software [35].

Measure	$V_{s,max}$(atom) (kJ mol^{-1})	Π (kJ mol^{-1})
P0RT	157.1(H) 33.8(I) 28.4(I) 19.9(I)	24.3
P0LT	124.1(H) 110.8(I) 110.4(I) 110.2(I)	36.0
P1RT	119.3(H) 110.3(I) 110.1(I) 108.1(I)	31.6
P2RT	114.0(H) 111.6(I) 110.8(I) 110.7(I)	32.0

The absolute maxima of the *Vs* (**r**) correspond to the most positive H atoms and the values on I atoms
correspond to the σ-holes. Maxima on hydrogen atoms are more influenced by the P-T changes, because the intermolecular interactions in which they are involved (hydrogen bonds) are more electrostatic with respect to the halogen bondings. In fact from **P0RT** disordered crystal structure to
P0LT, **P1RT** and **P2RT**, the *Vs,max*(H) value becomes significantly lower. On the other hand, halogen···halogen interactions reflect modifications in absolute value of electrostatic potential. Another interesting feature is the trend of the Π value: it strongly increases with phase transition as a
consequence of the formation of a net dipole moment in iodoform molecule and slightly decreases increasing pressure: this feature can be attributed to a reduction of dipole moment of the molecules due to a small and progressive squeezing of the the C-I3 "pyramid" in the *ab* crystallographic planes

Figure 8. V_s(**r**) in kJ mol^{-1} computed on 0.001e/bohr^3 charge density isosurface of CHI_3 molecule. Colors: red, V_s(**r**) more positive than 354.0, 354.0 > yellow > 189.12, 189.12 > green > 24.31 and blue less than 24.31.

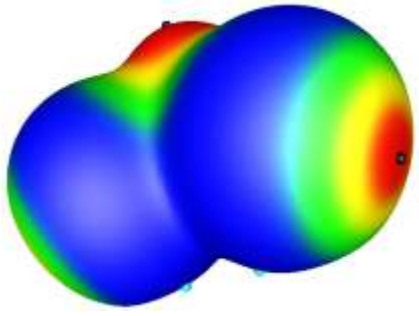

Cohesive energies computation. The shortening of intraplanar iodine···iodine interaction is mainly caused by the compression of the structure during high pressure experiments. However this is not only a geometrical feature; analyzing interaction energies, as is shown in Table 4, it is possible to understand how intermolecular interaction lead to crystal structures modifications under different P-T conditions.

Table 4. Computed interaction energy data (kJ mol^{-1}) for iodoform crystal.

	P0LT	**P1RT**	**P2RT**
***ΔE*/ kJmol^{-1} [a]**	-484.661	-520.109	-547.420
Grimme contribution/ kJmol^{-1}	326.410	344.258	358.026

[a] ΔE = E(bulk)/Z – E(mol-BSSE)

Increasing pressure cohesive energies of iodoform progressively increase, as well as Grimme dispersive contribution to the B3LYP energy and gradient and the computed sublimation enthalpy at 0 K; this means that the iodoform crystal structure compression gives rise to progressive stronger
intermolcular interactions.

Conclusions

At room conditions the polar CHI_3 molecules have the CH group disordered above and below the I_3
plane: therefore the structure is refined in the pseudo $P6_3/m$ space group and the plane of iodine atoms coincide with the crystallographic mirror plane. A disorder-order transition occurs in iodoform crystal structure increasing pressure at room temperature, passing to the polar and enatiomorphic $P6_3$ space group. The transition can be ascribed to the increased repulsion between disordered hydrogens due to the decreasing of distance among molecular planes caused by compression. The changes of pressure and temperature show the same geometrical effects on the CHI_3 crystal structure: under compression the cell volumes reduce monotonically, following the well known Birch- Murnagham trend. The effects of both thermodynamic condition changes are the same on halogen···halogen interactions: a progressive shortening occurs both for I···I interactions lying on molecular planes and for I···I among plane have been observed. This different polarization of the two iodoform phases has been be also demonstrated by the trend of the *Vs*(r) average absolute deviation for **P0RT**, **P0LT**, **P1RT** and **P2RT**. Moreover in **P1RT** and **P2RT** passing from room to high pressure, both hydrogen and halogen bonds become shorter and also stronger: this can be remarked by BSSE and Grimme corrected DFT/B3LYP cohesive energy calculations for iodoform experimental crystal structures.

Supplementary material. CCDC 911489 (**P0RT**), 911490 (**P1RT**) and 911491 (**P2RT**) contain the crystallographic data for this paper. These data can be obtained free of charge via http://www.ccdc.cam.ac.uk/conts/retrieving.html (or from the Cambridge Crystallographic Data Centre, 12, Uninion Road, Cambridge CB2 1EZ.UK; fax: +441223 336033).

Acknowledgments. The authors thanks ~~Dr.~~ Diego Gatta for the helpful suggestions about the ~~high pressure~~ HP experiments and the Scansetti Centre (University of Turin) for using Micro-Raman Spectrometer.

References and Notes

[1] G. Bao, D. Duan, F. Tian, L. Wang, B. Liu and T. Cui, J. Chem. Phys., 134 (2011) 034508-1.
[2] A. Samoc, M. Samoc, J. Giermanska, J. Sworakowski, H. Koiodziej, D.F. Williams, J. Phys., D18 (1985) 2529.
[3] D. Liu, W. Lei, G. Bao, F. Li, J. Hao, B. Liu, T. Cui, Q. Cui abd G. Zou, J. Phys. Chem., B113 (2009) 7430 *and references therein.*
[4] *a)*T.L. Khostsyanova, A.I. Kitaigorodskii and Y.T. Struchkov, Zh. Fiz. Khim., 27 (1953) 647; *b)*R.W.G. Wikoff, Crystal Structures, Vol. 5, Interscience, New York, 1964; *c)*A.I. Kitaigorodskii, T.L. Khostsyanova and Y.T. Struchkov, Dokl. Akad. Nauk SSSR, 78 (1951) 1161.
[5] Y. Iwata, T. Watanabe, Annu. Rep. Res. R.I. Kyoto U~~niv~~., 28 (1972) 967.
[6] N.V. Sidorov, Y.N. Krasyukov, E.I. Mukhtarova and D.M. Shkrabo, Crystallog. Rep., 45(2) (2000) 288.
[7] F. Bertolotti and G. Gervasio, J. Mol. Struct., 1036 (2013) 305
[8] A. Olejniczak, A. Katrusiak and A. Vij, CrystEngComm, 11 (2009) 1073.
[9] E.V. Boldyreva, Cryst. Eng., 6 (2003) 235.
[10] R.M. Hazen and R.T. Downs (Eds), Reviews in Mineralogy and Geochemistry, Mineralogical Society America and Geochemical Society, 41, Blacksburg, Virginia, 2000.
[11] N.V. Sidorov, Y. N. Krasyukov, E.I. Mukhtarova and D.M. Shkarabo, Crystallogr. Reports, 45(2) (2000) 288.
[12] Scansetti Center, University of Turin.
[13] H.K. Mao, J. Xu and P.M. Bell, Journal of Geophysical Research, 91 (1986) 4673.
[14] Agilent Technologies UK Ltd, Oxford, UK.
[15] Agilent Technologies, CrysAlisPro Software system, version 1.171.35.19, Agilent Technologies UK Ltd, Oxford, UK, 2012.
[16] R.J. Angel, J. Appl. Crystallogr., 37 (2004) 486.
[17] G.M. Sheldrick, Acta Crystallographica, A64 (2008) 112.
[18] Y. Iwata and T. Watanabe, Annu. Rep. Res. R.I,. Kyoto U., 7 (1979) 87.
[19] W.C. Hamilton, Acta Cryst., 18 (1965) 502.
[20] W. Kohn and L. Sham, J. Phys. Rev. A, 140 (1965) 1133.
[21] S. Grimme, J. Antony, T. Scwabe and F. Mück-Lichtenfeld, Org.Biomol.Chem., 5 (2007) 741.
[22] *a)*S. Grimme, J. Comput. Chem., 25 (2004) 1463; *b)*S. Grimme, J. Comput. Chem., 27 (2006) 1787.
[23] R. Dovesi, V.R. Saunders, C. Roetti, R. Orlando, C.M. Zicovich-Wilson, F. Pascale, B. Civalleri, K. Doll, N.M. Harrison, I.J. Bush, P. D'Arco and M. Llunell CRYSTAL09, University of Turin, Turin, Italy, 2010.
[24] *a)*N. Godbout, D.R. Salahub, J. Andzelm, and E. Wimmer, Can. J. Chem., 70 (1992) 560; *b)*S. Huzinga, E.J. Andzelm, M. Klobuski, E. Radzio-Andzelm, Y. Sakai, H. Takewaki, Gaussian basis set for molecular calculations, Elsevier, Amsterdam, 1984.
[25] S. F. Boys, F. Bernardi, Mol. Phys., 19 (1970) 553.
[26] K.F. Dziubek and A. Katriusiak, J. Phys. Chem. B, 112 (2008) 12001.

[27] J.J. McKinnon, M.A. Spackman and A.S. Mitchell, Acta Crystallogr., B60 (2004) 627.
[28] J.J. McKinnon, D. Jayatilaka and M.A. Spackman, Chem. Commun., (2007) 3814.
[29] CrystalExplorer 2.1 (381), S.K. Wolff, D.J. Grimwood, J.J. McKinnon, D. Jayatilaka, M.A. Spackman, University of Western Australia (http://hirshfeldsurface.net/CrystalExplorer/), 2005-2007.
[30] P. Metrangolo, F. Meyer, T. Pilati, G. Resnati and G. Terraneo, Angew. Chem. Int. Ed., 47 (2008) 6114.
[31] T.T.T. Bui, S. Dahaoui, C. Lecomte, G.R. Desiraju and E. Espinosa, Angew. Chem. Int. Ed., 48 (2009) 3838.
[32] *a)*A.V. Shishina, A.I. Stash, B. Civalleri, A. Ellern and V. G. Tsirelson, Mendeleev Comm., 20 (2010) 161; *b)* Y.V. Nelyubina, M.Y. Antipin, D.S. Dunin, V.Y. Kotov and K.A. Lyssenko, Chemm. Comm., 46 (2010) 5325.
[33] *a)*A. Anthony, G.R Desiraju, S.S. Kuduva, N.N.L. Madhavi, A. Nangia, R. Thaimattam, V. R. Thalladi, Cryst. Eng., 1 (1998) 1; *b)*R.K.R. Jetti, F. Xue, T.C.W. Mak, A. Nangia, Cryst. Eng., 2 (1999) 215; *c)*E. Bosch, C.L. Barnes, Cryst. Growth Des., 2 (2002) 299; *d)*B.K. Saha, R.K.R. Jetti, L.S. Reddy, S. Aitipamula, A. Nangia, Cryst. Growth Des., 5 (2005) 887; *e*)V.R. Hathwar, T.N.J. Guru Row, Phys. Chem., A114 (2010) 13434; *f)*M. Solimannejad, M. Malekani, I.J. Alkorta, Phys. Chem., A114 (2010) 12106.
[34] *a)*G. Trogdon, J.S. Murray, M.C. Concha and P. Politzer, J. Mol. Model., 13 (2007) 313; *b)* T. Brinck, J.S. Murray, P. Politzer, Mol. Phys., 76 (1992) 609.
[35] WFA v1.0: A wavefunction analysis program written by Dr. Felipe Bulat. F. A. Bulat and A. Toro-Labbe, WF: A suite of program to analyse wavefunctions, unpublished; F.A. Bulat, A. Toro-Labbe, T. Brink, J.S. Murray and P. Politzer, J. Mol. Mod. (2010).